chemistry

MDPI

Article

Breathable Iron-Based MIL-88 Framework as Dye Adsorbent in Aqueous Solution

Dita A. Nurani [1,2], Nabila Anisa [1,2,†], Irena Khatrin [1,2,†], Yasmine [1,2], Grandprix T. M. Kadja [3,4,5] and Yuni K. Krisnandi [1,2,*]

[1] Department of Chemistry, Faculty of Mathematics and Natural Science, Universitas Indonesia, Depok 16424, Indonesia; d.arifa@sci.ui.ac.id (D.A.N.); nabilaanisaa30@gmail.com (N.A.); irena.khatrin@sci.ui.ac.id (I.K.)
[2] Solid Inorganic Framework Laboratory, Department of Chemistry, Faculty of Mathematics and Natural Science, Universitas Indonesia, Depok 16424, Indonesia
[3] Division of Inorganic and Physical Chemistry, Faculty of Mathematics and Natural Sciences, Institut Teknologi Bandung, Jalan Ganesha No. 10, Bandung 40132, Indonesia; grandprix.thomryes@itb.ac.id
[4] Center for Catalysis and Reaction Engineering, Institut Teknologi Bandung, Jalan Ganesha No. 10, Bandung 40132, Indonesia
[5] Research Center for Nanosciences and Nanotechnology, Institut Teknologi Bandung, Jalan Ganesha No. 10, Bandung 40132, Indonesia
* Correspondence: yuni.krisnandi@sci.ui.ac.id; Tel.: +62-812-1856-7060
† These authors contributed equally to this work.

Abstract: Metal–organic frameworks (MOFs) have been observed to exclusively eliminate dyes confined within their respective pores. In this investigation, the synthesis of a breathable MOF structure, MIL-88B(Fe), was pursued with the objective of circumventing restrictions on pore size to enhance its adsorption capabilities. The synthesis of MIL-88B(Fe) was carried out via the assisted solvothermal method at 373 K using inexpensive yet environmentally benign $FeCl_3 \cdot 6H_2O$, 1,4-benzenedicarboxylic acid, and DMF as a metal precursor, linker, and solvent, respectively. Furthermore, the MOF was subjected to extensive analytical characterisation using XRD, FT-IR spectroscopy, N_2 gas sorption, TGA, and SEM. The experimental data showed that the utilisation of MIL-88B(Fe) with a dose level of 5 mg for 180 min at a pH of 9 led to the highest levels of adsorption for both dyes, with 162.82 mg g^{-1} for methylene blue (MB) and 144.65 mg g^{-1} for rhodamine B (RhB), as a result of the contrast in the molecular size between each dye. The Langmuir and Freundlich models demonstrated a correlation with isotherms, while the thermodynamic analysis demonstrated that MIL-88B(Fe) exhibits distinct endothermic and breathable properties. The efficacy of MIL-88B(Fe) adsorbent for MB and RhB in aqueous solutions indicated exceptional performance, stability, and noteworthy reusability performance.

Keywords: metal–organic framework; Fe-MOF; breathable adsorbent; dye removal; MIL-88B(Fe)

Citation: Nurani, D.A.; Anisa, N.; Khatrin, I.; Yasmine; Kadja, G.T.M.; Krisnandi, Y.K. Breathable Iron-Based MIL-88 Framework as Dye Adsorbent in Aqueous Solution. *Chemistry* **2024**, *6*, 283–298. https://doi.org/10.3390/chemistry6020015

Academic Editor: Emmanuel Unuabonah

Received: 20 December 2023
Revised: 28 February 2024
Accepted: 4 March 2024
Published: 14 March 2024

1. Introduction

The residual dyes from the textile, pharmaceutical, pulp, and paper industries have caused serious problems for the environment and the health of living beings due to their toxicity and carcinogenicity. In the textile industry, organic dyes are frequently used to create a variety of colours and textures. These reactive, non-degradable dyes, including methylene blue, Congo red, and rhodamine B, often lose 10–20% of their concentration in wastewater [1,2]. A variety of methodologies have been employed for the elimination of organic dye effluent from aqueous solutions, including, but not limited to, chlorination, electrochemical treatment, photodegradation, coagulation, and adsorption [3–7]. Among the various techniques available for the elimination of organic colourants from large-scale aqueous environments, adsorption using a range of adsorbent materials is highly regarded due to its numerous advantages. These benefits include ease of preparation and operation,

high economic value, remarkable efficiency, and suitability for a wide range of dyes. Studies imply that adsorption using diverse adsorbents works as an alternative for the elimination of organic colourants from large water bodies [8–10]. Materials such as clay, zeolites, activated carbons, and metal–organic frameworks (MOFs) have demonstrated their efficacy in the adsorption of both pollutants and organic dyes, as evidenced by previous studies [11–16].

Organic ligands and metal ions that play roles as linkers and metal node precursors, respectively, in the synthesis of porous-material MOFs have been employed for diverse applications like catalysis, gas separation, and environmental remediation [1,17–20]. MOFs have been extensively researched owing to their exceptional features, including their outstanding surface area as a result of their porous features with regulated pores and huge cavity sizes that are structured in an orderly manner [5–8]. The features and qualities of MOFs are influenced by the framework design and various synthesis techniques. As reported by Li et al., MIL-53 has exhibited a strong adsorption capacity in the elimination of malachite green and methylene blue dyes [21]. Reactive hazardous dyes like reactive yellow 15 and red 25 have been effectively removed by MIL-101 [1]. NH_2-MIL-88(Fe) has been reported to be an effective adsorbent for removing Congo red via chemisorption [22], while He et al. used NH_2-MIL-88B(Fe) as a peroxide-like catalyst for the Fenton-like degradation of methylene blue, with both studies demonstrating outstanding adsorption stability and a straightforward regeneration process [23].

The thermal stability of MOFs is a consequence of the robust nature of the metal ions and ligand-bonding interactions. Numerous metallic ions in MOFs have been investigated in research concerning the adsorption and elimination of organic dyes, including Al-MOF, Zn-MOF, Cu-MOF, Cr-MOF, Y-MOF, Co-MOF, and Fe-MOF [1,24–31]. Based on our earlier findings, several transition-metal-based MOFs have been described. For instance, high-thermal-stability Co-MOF and high-surface-area Y-MOF crystalline demonstrated excellent performance as adsorbents for rhodamine B and methylene blue, respectively [32,33]. Transition metals have been reported to enhance the physicochemical properties of the as-synthesised MOF. However, many transitional metals, including noble metals, are relatively expensive and do not meet the requirements for use on an industrial scale. Therefore, we are keen to report the synthesis of MOFs using abundant and inexpensive transition metals. The semiconductor characteristics, strong catalytic activity, and stability of iron (Fe) have generated a great deal of attention. It is also non-toxic, and is the cheapest and one of the most abundant metals. The oxidation number of metal ions also contributes to the force of electrostatic attraction, which holds the whole structure of the MOF together. The ligands in MOF structures are said to form strong connections with trivalent metal ions [34]. In a prior publication, we described a single-step process for replacing the Cr^{3+} ions in MIL-101 with Fe^{3+} and Sc^{3+}, which produced the polymorphic MOF MIL-88B with a somewhat low-stability structure [35].

MOFs have been identified as a potential technology for dye adsorption in water treatment. However, recent studies by Uddin et al. revealed that the inconsistent and stable trait of the pore size in MOFs presents a significant obstacle to the efficient utilisation of MOFs in this context [24]. MOFs typically only apply to dyes with particle sizes smaller than the MOF's pore size and volume. Large-particle dyes cannot be effectively removed from aqueous solutions by MOFs with relatively low pore sizes, while MOFs with large pore sizes are not selective enough to remove small-particle dyes from aqueous solutions. Numerous MOFs have been thoroughly developed with flexible and dynamic features to enhance their potential applications. The one-dimensional channels as a building block of the MOF may reversibly lengthen or shorten depending on thermodynamic variables like temperature, pressure, or trapped molecules [36,37]. Volringer et al. and Chaplais et al. described how the flexibility feature, known as the breathing effect, depends on the metal centre of MOFs [38,39]. For instance, MIL-53(M) MOFs, denoted by *M* as metals such as Al, Ga, Fe, Cr, Sc, and In, can breathe due to their flexible diamond-shaped scaffolds [36]. Meanwhile, Surblé et al. developed a series of MIL-88 metal–organic frameworks that consist of hexagonal, six-connected breathable network structures [40].

The current work involved the replacement of Cr^{3+} in MIL-101 with inexpensive and environmentally benign Fe^{3+}, which produced MIL-88B(Fe). Eco-friendly metal Fe and BDC ligands were used in a one-step solvothermal synthesis process with DMF. The MIL-88B(Fe) material was then subsequently employed as an adsorbent to eliminate dyes from aqueous solutions. Cationic dyes with differences in particle size, including MB (methylene blue) and RhB (rhodamine B), which are larger-molecular-size dyes, as depicted in Figure 1, were employed as model compounds to signify the flexibility properties of the as-synthesised MOF. The optimal adsorption environments, including the initial dye dose, contact time, pH, and adsorption-related variables such as isotherms, kinetics, and thermodynamics, were investigated. Furthermore, the reusability and selectivity against two cationic dyes of MIL-88B(Fe) were investigated.

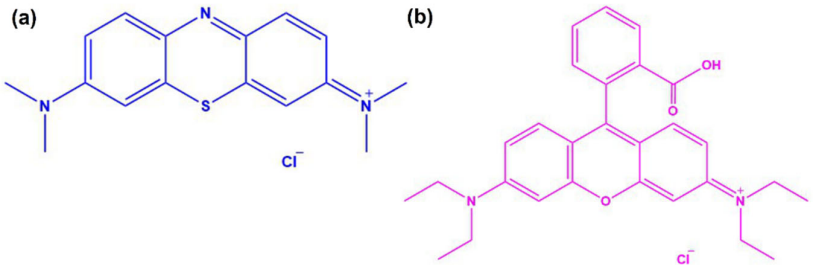

Figure 1. Chemical structure of MB (**a**) and RhB (**b**).

2. Materials and Methods

2.1. Materials

The chemicals utilised in this report were all purchased from Sigma Aldrich (St. Louis, MO, USA), including iron (III) chloride hexahydrate ($FeCl_3 \cdot H_2O$, ACS reagent, 97%), terephthalic acid (1.4-benzenedicarboxylic acid, 98%), DMF (*N*,*N*-dimethylformamide, anhydrous, 99.8%), MB (methylene blue, ≥95%), and RhB (rhodamine B, ≥95%), as well as sodium hydroxide (NaOH, pellets EMPLURA®), acetic acid (CH_3COOH, glacial, ReagentPlus®, ≥99%), and ethanol absolute (CH_3CH_2OH, for analysis EMPARTA® ACS). All substances were utilised in their original form without any purification. The solvent employed for the adsorption experiments was distilled water.

2.2. Synthesis of MIL-88B(Fe)

The synthesis of the MIL-88B(Fe) MOF was carried out using the methodology reported by Zhu et al., with some modifications [7]. Mixtures of 4.9 mmol and 2.5 mmol of iron (III) chloride hexahydrate and 1,4-benzenedicarboxylic acid, respectively, were obtained by dissolving the reagents in 30 mL of dimethylformamide (DMF) with continuous stirring for 30 m. Subsequently, the mixture was crystallised for 20 h in the oven using a 50 mL autoclave lined with Teflon at 373 K. The resultant product was subjected to two rounds of ethanol washing at 333 K for a duration of 3 h each to eliminate any unreacted material. Subsequently, it was heated at 333 K for 24 h.

2.3. Characterisation of MIL-88B(Fe)

Fourier-transform infrared (FT-IR) spectrometry was performed on an Alpha Bruker (Rheinstetten, Germany) under the KBr method (4 cm^{-1} resolution) to analyse the functional groups within the MOF. A PANanalytical (Malvern, UK): X'Pert Pro XRD was utilised to record the XRD patterns under the radiation of Cu-Kα at 40 kV and 30 mA (λ = 1.54184 Å). The surface area of the MOF was evaluated using the Brunauer–Emmett–Teller (BET) method on a Surface Area Analyzer (SAA) Quantachrome-Evo Surface Area and Pore Size Analyzer (Boynton Beach, FL, USA) with N_2 at 77 K. The t-plot method was applied to determine the external surface area and micropore volume. The total pore volume was measured from the amount of N_2 adsorbed at P/P_0 = 0.99. The Quanta 650 Scanning Electron Microscope (Hillsboro, OR, USA.) was used at 20 kV to examine the morphologies

of the MOF. Thermogravimetric Analysis (TGA) was carried out using Thermogravimetric–Differential Thermal Analysis LINSEIS STA Platinum Series instruments (New Castle, DE, USA) at a 10 °C/min heating rate with N_2 flow.

2.4. Adsorption Experiments

MB and RhB, two organic cationic compounds that varied in molecular size, were chosen as the models to evaluate the efficacy and breathing impact of MIL-88B(Fe) materials. Here, 5 mg of MIL-88B(Fe) was applied to 5 mL of 5 mg L^{-1} MB and RhB. The adsorption experiments were conducted for 120 min at room temperature. The respective concentrations of MB and RhB dyes were then ascertained by an ultraviolet–visible (UV-Vis) spectrophotometer (T92+, PG Instruments) (Leicestershire, UK) at λmax = 554 and 664 nm. The adsorption capacity at a certain time (q_t, mg g^{-1}) and equilibrium (q_e, mg g^{-1}) was determined from the following equation:

$$q_t = \frac{(C_0 - C_t)V}{m} \quad (1)$$

$$q_e = \frac{(C_0 - C_e)V}{m} \quad (2)$$

where C_0, C_t, and C_e are the initial dye concentrations (mg L^{-1}) at equilibrium and certain time t, respectively. m is described as the adsorbent mass (g), and V is the volume of dye solution (L).

3. Results and Discussion

3.1. Synthesis and Characterisation of MIL-88B(Fe)

The synthesis of MIL-88B(Fe) is based on our prior study with the idea of replacing the Cr^{3+} ions in MIL-101 with Fe^{3+} as an inexpensive yet environmentally benign metal [35]. Therefore, to improve the stability of the as-synthesised MIL-88B(Fe), the synthesis was carried out using the method disclosed by Zhu et al., with some modifications via the assisted solvothermal method at 373 K [7]. Figure 2a depicts the XRD pattern of the resulting MIL-88B(Fe). According to the study conducted by Zhu et al. on their synthesis of MIL-101(Fe), which is the method followed with modifications in this paper, MIL-101 possesses characteristic diffraction peaks at 2θ = 3.3°, 6.9°, and 7.3° (CCDC No. 605510) [7]. While the as-synthesised MOF XRD pattern exhibited diffraction peaks at 2θ = 9.0°, 9.7°, 10.0°, 16.5°, and 16.8°, some new phases also appeared at 2θ = 9.4°, 12.5°, and 18.6°, corresponding to MIL-88B, which is the framework isomer of MIL-101 [35]. The Rietveld refinement approach was carried out for the reference (CCDC No. 1892483), and the experimental XRD patterns of MIL-88B(Fe) with the structural formula of $[Fe_3O(OH)(BDC)_3(H_2O)_2]$, based on a triclinic structure with a P-1 space group (Figure S1), revealed a goodness of fit (defined by $G = \chi^2$) of 1.068. These results indicate the effective creation of MIL-88B(Fe), which is supported by the well-fitted diffraction of the reference and experimental data [1,41]. The modifications to the synthesis technique, such as raising the temperature, extending the reaction time, and altering the ratio of the precursors in comparison to MIL-101, may have an impact on these alterations in the framework structure [42].

Figure 2b presents the FT-IR spectra of the resulting MOF, with $FeCl_3 \cdot 6H_2O$ as the metal precursor and 1,4-benzenedicarboxylic acid as the linker. The MOF exhibits absorption peaks at 3520 and 2950–2935 cm^{-1}, relating to the functional group of O–H stretching and C–H sp^2, respectively. Adsorption peaks at 1672 and 1380–1450 cm^{-1} correspond to C–H bending as well as asymmetric and symmetric C–O stretching of carboxylate groups [43]. Furthermore, absorption peaks were observed at 600–500 cm^{-1} owing to Fe–O band vibrations with metal precursors. A slight shift of the C=O peaks of the organic linker, both asymmetric and symmetric vibrations, to the lower wavenumber at 1672 cm^{-1} indicated the bond between the linker and metal of MIL-88B(Fe), confirming the XRD results.

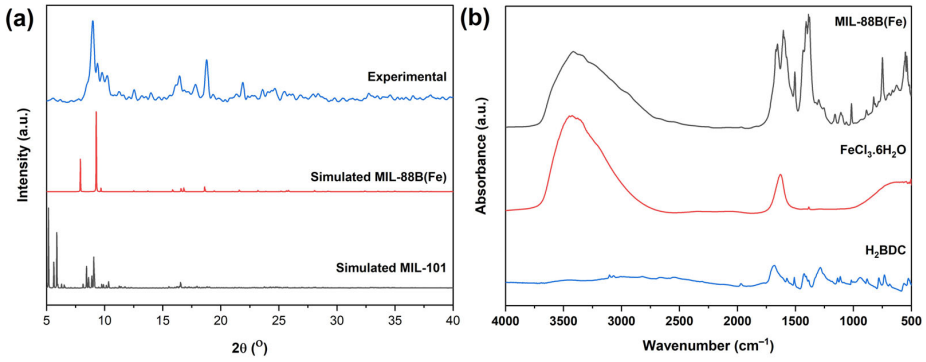

Figure 2. XRD patterns (**a**) and FT-IR spectra (**b**) of MIL-88B(Fe).

According to the SEM analysis, MIL-88B(Fe) exhibits an octahedral structure (Figure 3a,b) similar to that of a conventional crystalline and porous Fe-based MOF reported by Zhu, T. et al. and Taylor-Pashow et al. [7,17,44]. The EDX spectrum of MIL-88B(Fe) (Figure S2) reveals the existence of peaks of C, O, Fe, and Cl elements, which are detailed in Table 1. Moreover, the SEM elemental mapping images (Figure 3c) confirm the homogeneous dispersion of each element in MIL-88B(Fe). Figure S3 illustrates the N_2 physisorption isotherm and BJH pore size distribution of the resulting MIL-88B(Fe), which shows a very low BET surface area of 28.37 m^2 g^{-1}, a pore volume of 0.248 cm^3 g^{-1}, and an average pore diameter of 6.2 nm (Table 1). These results are similar to those of our previous study (BET surface area of 16 m^2 g^{-1}) and other reported studies of MIL-88B(Fe), such as Rahmani et al. and Vuong et al., with a BET surface area of 23 m^2 g^{-1} and 30 m^2 g^{-1}, respectively [35,45,46].

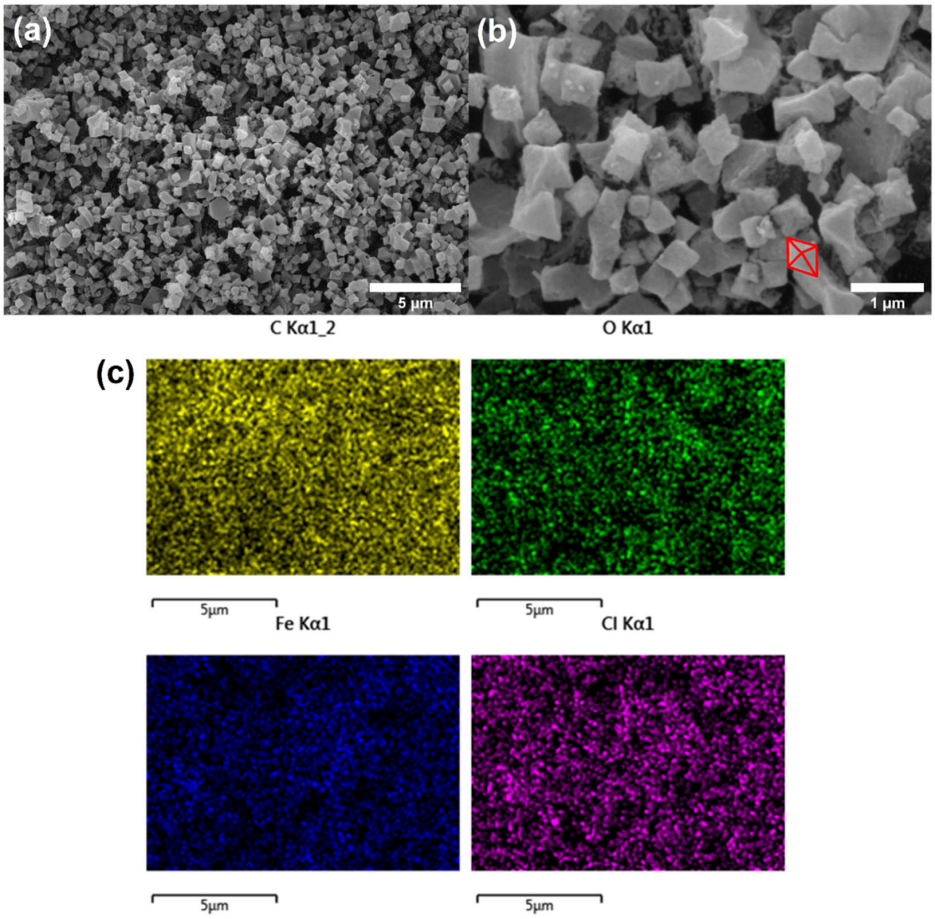

Figure 3. SEM images (**a**,**b**) and corresponding elemental mapping images (**c**) of MIL-88B(Fe).

Table 1. Physicochemical properties of MIL-88B(Fe).

S_{BET} (m^2 g^{-1}) [a]	V_{Total} (cm^3 g^{-1}) [b]	Avg. Pore Diameter (nm) [c]	% Wt. [d]			
			C	O	Fe	Cl
28.37	0.248	6.20	61.8	25.4	10.8	2.0

[a] Determined using the BET method. [b] Determined at $p/p_0 = 0.99$. [c] Determined using the BJH method. [d] Determined using EDX.

MIL-88B(Fe) was evaluated for thermal stability using TGA from 25 °C to 750 °C (Figure 4a). Five plateaus were detected in the TG curve. Here, 16.9% of the weight loss at 90–120 °C indicates the evaporation of H_2O molecules, while the second minor plateau between 120 °C and 300 °C may be attributed to DMF solvent evaporation. Finally, the latter plateaus between 300 °C and 700 °C are linked to the breakdown of an organic framework with a mass loss of 40%, which corresponds to two BDC linkers used in the synthesis, which leads to the fabrication of iron oxide at 750 °C. The mass reduction is in agreement with the original formula of the crystal as $[Fe_3O(OH)(BDC)_3(H_2O)_2]$, which is consistent with earlier findings by [11]. The DTA analysis in Figure 4b reveals an endothermic peak below 120 °C with minor weight loss. The significant weight loss corresponds well with the DTA results by the appearance of two exothermic peaks at around 360 °C and 680 °C as a result of the loss of organic fragments and confirms the stability of MIL-88B(Fe) up to 300 °C.

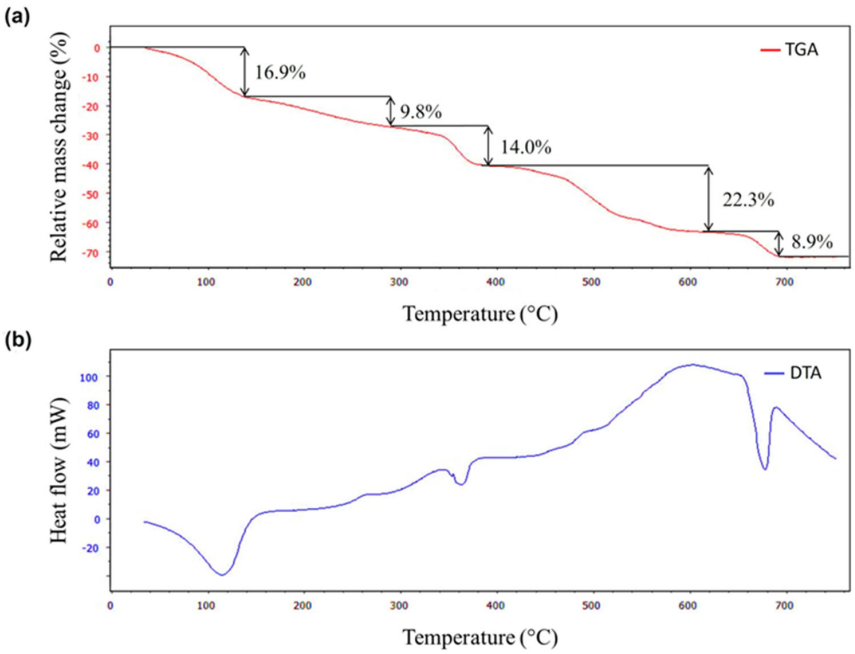

Figure 4. (**a**) TGA and (**b**) DTA profile of MIL-88B(Fe).

3.2. Adsorption Experiments

MIL-101(Cr), the original MOF framework in which Cr^{3+} ions were substituted with Fe^{3+} to produce MIL-88B(Fe), is a poor MB and RhB adsorbent [35]. As a result, several modifications, such as the inclusion of mineralising agents, morphological changes, and MOF hybridisation into composites, have been reported with the aim of improving the adsorption performance of MIL-101(Cr) [47–50]. However, none of the aforementioned methods demonstrated better adsorption towards both MB and RhB, while amino-functionalised MIL-101(Cr) has been shown to provide better adsorption towards RhB than MB [51]. Therefore, the as-synthesised MIL-88B(Fe), which is known for its breathable structure, was evaluated as an adsorbent in the removal of two distinct-size dyes, MB and RhB.

3.2.1. Effect of pH

The impact of initial pH on the MIL-88B(Fe) adsorption of MB and RhB was investigated in the pH range of 3 to 12. The findings are presented in Figure 5a. The adsorption capacity of MIL-88B(Fe) towards MB and RhB increased gradually when the pH was altered from 3 to 9 and decreased at pH 12. The optimum adsorption capacity of MIL-88B(Fe) was observed at pH 9. This could be due to the electrostatic interaction that regulates the adsorption of MB and RhB. The positive charge density of MIL-88B(Fe) increased at an acidic pH, which reduced the adsorption of cationic dyes, as explained by electrostatic repulsion. In addition, excess H^+ ions in the solution were observed to compete with cationic dyes for the active sites of MIL-88B(Fe), causing a decrease in adsorbed dyes [21]. On the other hand, at pH 9, the negative charge density of MOF expanded due to the deposition of OH^- ions on the MIL-88B(Fe) surface. It showed high adsorption capacity for the positively charged cationic dyes through electrostatic interaction. At a basic pH, the hydroxyl groups (O–H) and carbonyl groups (C=O) on the external area of the MOF attracted the cationic dye compounds [52]. Furthermore, at pH >9, the adsorption capacity decreased significantly. Previous research also reported that the optimum pH of Co-MOF and Fe-MOF with the succinic acid linker to absorb MB is pH 9 [33]. This condition was necessary because MIL-88B(Fe)'s structure might disintegrate and begin to hydrolyse in a strongly basic solution [21].

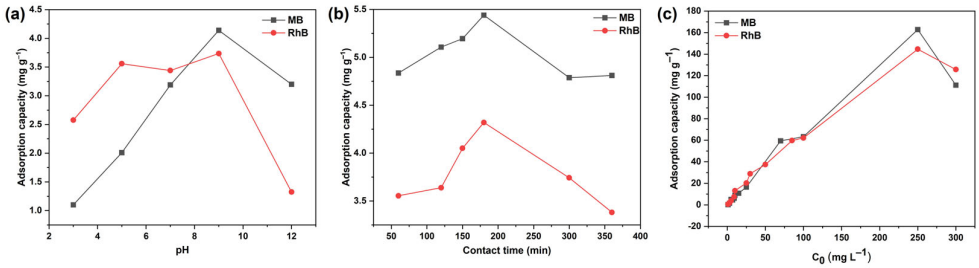

Figure 5. Effect of pH (**a**), contact time (**b**), and initial dye concentration (**c**) on the adsorption capacity of MIL-88B(Fe) towards MB and RhB.

3.2.2. Effect of Contact Time

Figure 5b demonstrated the impact of contact time on the adsorption of dyes by MIL-88B(Fe), which was examined at 60 to 360 min time intervals at pH 9. The adsorption profile was observed to be similar for both cationic dyes and comprised two phases. The first phase occurred at 60–180 min, owing to the adsorption of MB and RhB with an initial dose of 5 mg L^{-1} to reach the equilibrium adsorption state. The adsorption capacity, q value, expanded rapidly over time due to a tremendous number of active sites on the external area of MIL-88B(Fe). The second adsorption phase started once the binding between the dyes (MB and RhB) and MIL-88B(Fe) adsorbent was complete and achieved the equilibrium state where the surface of MOF became fully occupied and saturated. However, the adsorption capabilities significantly decreased after 180 min of contact time, indicating the leaching of dye molecules over time due to a weakening of the interaction between the dyes and the MOF.

3.2.3. Effect of Initial Dye Concentration

Figure 5c illustrates the increments in the adsorption capacity of MIL-88B(Fe) towards both MB and RhB dyes as the initial dye concentration increased and became saturated at 250 mg L^{-1}. Due to a lack of active sites, an increase in dye concentration would result in a reduction in dye removal [52]. According to the findings under optimum circumstances, the optimal MOF capacity on MB and RhB was 162.82 mg g^{-1} and 144.65 mg g^{-1}, respectively. This suggests that the molecular size of the dyes also affects the adsorption process. Since RhB possesses a greater molecular size (~1.77 nm) compared to MB (~1.40 nm), it might limit the penetration process of RhB into the pores on the MIL-88B(Fe) surface.

3.2.4. Adsorption Isotherms

The MB and RhB adsorption isotherms on MIL-88B(Fe) under the ideal adsorption conditions of pH 9, contact period of 180 min, and starting dye concentration of 250 mg L^{-1} are depicted in Figure 6a,b. The Langmuir and Freundlich models were fitted as the typical models for liquid-phase adsorption.

$$\frac{C_e}{q_e} = \frac{1}{K_L q_{max}} + \frac{C_e}{q_{max}} \quad (3)$$

Equation (3) represents the Langmuir isotherm equation, with C_e (mg L^{-1}) denoting the equilibrium solute concentration, q_{max} denoting the maximum amount of adsorption, and K_L (L mg^{-1}) denoting the Langmuir adsorption constant related to the adsorption binding energy [21]. Adsorption is thought to be a monolayer process, according to the Langmuir model. The nonlinear fitting of C_e/q_e vs. C_e (Figure 6a) may be used to determine the values of R^2, the adsorption capacity (q_{max}), and Langmuir constants (K_L), where a large K_L value indicates a favourable adsorption process. The adsorption isotherm constants are listed in Table 2. Both MB and RhB exhibit an R^2 value of >0.99 when the Langmuir isotherm model is fitted. At concentrations between 1 and 9 mg L^{-1}, the q_{max} value of RhB was found to be higher than that of MB, but decreased as the concentration increased. Furthermore, it was observed that the adsorption capacity of MB was higher than RhB, as depicted by the higher q_{max} value of MB (218.94 m g^{-1}) than RhB (167.67 m g^{-1}).

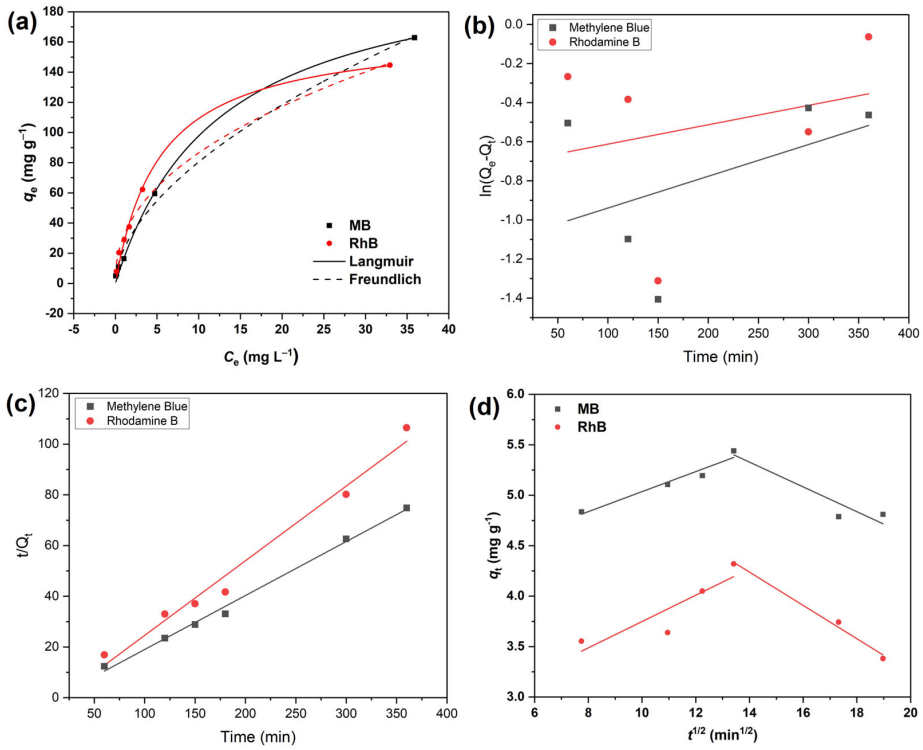

Figure 6. Nonlinear fitting of Langmuir and Freundlich isotherm models (**a**), linear-fitting kinetics by pseudo-first-order (**b**) and pseudo-second-order (**c**), and intraparticle diffusion models (**d**) of MB and RhB.

Table 2. Langmuir and Freundlich isotherm constants of MIL-88B(Fe).

Dyes	Langmuir Model			Freundlich Model		
	q_{max} (mg g^{-1})	K_L (L mg^{-1})	R^2	1/n	K_F	R^2
MB	218.94	0.0807	0.9975	0.5583	22.36	0.9953
RhB	167.67	0.1870	0.9935	0.4392	31.46	0.9895

Furthermore, the adsorption isotherm results were also fitted with the Freundlich model (Figure 6a), as follows:

$$q_e = K_F C_e^{\frac{1}{n}} \quad (4)$$

where K_F is the Freundlich constant, and n is correlated with the adsorption strength [27]. The Freundlich isotherm presumptively includes both monolayer and multilayer adsorption in heterogeneous adsorption. Both MB and RhB adsorption are well fitted to the Langmuir model, as evidenced by the higher R^2 value. Therefore, it is proposed that MB and RhB adsorption are confined to a monolayer and the adsorption sites are homogeneous. The adsorption of MB on the surface of Fe-MOF (succinic acid ligand) has also been studied in the past to fit the Langmuir model [33]. However, the R^2 of the Freundlich model concurs with the experimental findings of MB and RhB adsorption ($R^2 > 0.98$), suggesting that the bond between both cationic dyes and the external area of MIL-88B(Fe) is not entirely monolayer adsorption. A small number of heterogeneous adsorptions may also exist, and the driving force may come from chemical adsorption [33].

3.2.5. Adsorption Kinetics

The adsorption process and behaviour of the dyes were examined by fitting the kinetic experimental data to pseudo-first-order and pseudo-second-order kinetic models (Figure 6c,d) [53]. The rate constants of pseudo-first-order (k_1) and pseudo-second-order (k_2) kinetics may be obtained from the fitted data [54]. The pseudo-first-order kinetic model (Figure 6c) presupposes that adsorption is a diffusion-controlled process, with the adsorption rate being defined as the difference between the equilibrium and time-dependent adsorption capacities [55]. The pseudo-first-order formula is as follows:

$$\ln(q_e - q_t) = \ln q_e - k_1 t \quad (5)$$

where q_t (mg g^{-1}) is the quantity of the adsorbent that was adsorbed at time t (min), and q_e (mg g^{-1}) is the amount of adsorption that was present at equilibrium. In contrast, the pseudo-second-order model (Figure 6d) postulates that adsorption occurs because of electron sharing or transfer between adsorbents or is simply referred to as chemical adsorption [54]. The pseudo-second-order kinetic model formula is:

$$\frac{t}{q_t} = \frac{1}{k_2 q_e^2} - \frac{t}{q_e} \quad (6)$$

Table 3 displays the kinetic parameters as well as the correlation coefficients (R^2). The pseudo-second-order kinetic model provides the best fit based on linear fitting in comparison to nonlinear fitting (Figure S4) for the adsorption of the dyes MB and RhB, indicating that the rate-determining step is chemisorption based on the higher correlation coefficient values of the pseudo-second-order compared to the pseudo-first-order and the value of the second dynamic adsorption (q_{cal}), which is not far from the experimental value (q_{exp}) [56].

The intraparticle diffusion was also studied to analyse the adsorption process by fitting the kinetics data to the formula:

$$q_t = k_i t^{\frac{1}{2}} + c \quad (7)$$

where k_i is the intramolecular diffusion constant and c (mg g^{-1}) is a constant. The multilinear graphs, as shown in Figure 6d, reveal that the adsorption of MB and RhB occurred in two-step stages. The initial phase is the film diffusion model, which describes how dye molecules distribute from a mixture to the interlayered external area of the adsorbent. The second phase is the intraparticle diffusion phase, which is the diffusion of dyes into the porous system of the adsorbent [57,58]. The intraparticle diffusion model is suitable for the analysis of both MB and RhB adsorption on MIL-88B(Fe), and the strong correlation coefficient demonstrates that the rate-controlling step for MB and RhB is the diffusion of dyes into the adsorbent pores [59].

Table 3. Adsorption kinetics parameters of MB and RhB adsorption.

Dyes	Parameters	Dyes	
		MB	**RhB**
Pseudo-second-order model	q_{cal} [a] (mg g^{-1})	4.70	3.40
	q_{exp} [b] (mg g^{-1})	5.44	2.76
	k_2 (g mg^{-1} min^{-1})	1.99×10^{-2}	1.78×10^{-2}
	R^2	0.9951	0.9808
Pseudo-first-order model	q_{cal} [a] (mg g^{-1})	0.3324	44.456
	k_1 (min^{-1})	1.6×10^{-3}	6.0×10^{-4}
	R^2	0.213	0.0971
Intraparticle diffusion models	k_{i1} (mg g^{-1} $min^{-1/2}$)	0.10	0.13
	C_1 (mg g^{-1})	4.04	2.44
	R^2	0.9491	0.7908
	k_{i2} (mg g^{-1} $min^{-1/2}$)	0.12	0.17
	C_2 (mg g^{-1})	7.05	6.55
	R^2	0.8981	0.9906

[a] $q_{e,exp}$ is the equilibrium adsorption capacity in accordance with the experiments. [b] $q_{e,cal}$ is determined in accordance with the linear fitting from the kinetic models.

3.2.6. Adsorption Thermodynamics

The thermodynamic study was conducted at temperatures of 298, 308, and 318 K, with the findings shown in Table 4, to further analyse the adsorption behaviour of MB and RhB on MIL88(Fe). The thermodynamic parameters analysed were the adsorption enthalpy change (ΔH°), the Gibbs free energy change (ΔG°), and the entropy (ΔS°), where each is indicative of the system's heat content, the reaction spontaneity, and the disordered degree of the adsorption process, respectively, calculated by [55]:

$$\ln\left(\frac{q_e}{C_e}\right) = -\frac{\Delta H^\circ}{RT} + \frac{\Delta S^\circ}{R} \quad (8)$$

$$\Delta G^\circ = \Delta H^\circ - T\Delta S^\circ \quad (9)$$

where the absolute temperature and the universal gas constant are denoted as T (K) and R (8.314 J mol^{-1} K^{-1}), respectively. The positive value of ΔH° reveals that the adsorption process of MB and RhB is endothermic, where the performance of the adsorption is especially influenced by an elevation in temperature. The positive value of ΔS° implies an increase in entropy reduction and system chaos reduction in the adsorption processes of MB and RhB. The degree of freedom of the system was raised by the adsorption of additional solute molecules [54]. Meanwhile, the ΔG° value of MB ($\Delta G^\circ < 0$) and RhB shows a slight difference, as RhB only possessed $\Delta G^\circ > 0$ at T = 318 K, which implies that the adsorption of MB is spontaneous even under ambient conditions, unlike the adsorption of RhB that happens spontaneously at T = 318 K or higher. These results are supported by the fact that the molecular size of RhB (~1.77 nm) is larger than that of MB (~1.40 nm). However, the adsorption still happens spontaneously at T > 318 K, which confirms the breathable characteristic possessed by MIL-88B(Fe) due to the flexibility of the pores (Ø6.2 nm) to expand and accommodate RhB molecules.

Table 4. Thermodynamic parameters of MB and RhB adsorption.

Dyes	T (K)	ΔG° (kJ/mol)	ΔH° (kJ/mol)	ΔS° (J/mol/K)
MB	298	–2.42	42.98	152.30
	308	–3.95		
	318	–5.47		
RhB	298	1.65	28.17	88.95
	308	0.76		
	318	–0.12		

3.2.7. Reusability

Reusability is an important factor for an effective adsorbent in large-scale applications. The mixture of solvent elutions was adopted from previous research [33]. MIL-88B(Fe) was regenerated by a simple process for 30 min until the solution became completely clear. The reusability of MIL88B(Fe) was analysed under the conditions of 50 mg L^{-1}, pH 9, and a contact time of 180 min. In this study, three-cycle experiments were conducted using regenerated MIL-88B(Fe). The effect of the regeneration cycle is depicted in Figure 7a. In comparison with fresh MIL-88B(Fe), the adsorption capacity on MB decreased by <10% in the second cycle, and after three cycles, the adsorbent capacity was reduced by 11.46%, but remained at a high value (82.76%). This reveals an enhanced stability of MIL-88B(Fe) on MB adsorption. The adsorption capacity of MIL-88B(Fe) on RhB decreased by 10.37% from 82.76% to 72.41% in the second cycle, and it decreased significantly from 72.41% to 41.47% in the third cycle. The results showed that the reusability of MIL-88B(Fe) towards MB adsorption was greater than for RhB adsorption. The molecule size effect and bond strength between MIL-88B(Fe) and RhB may restrict the leaching process. The addition of strong acid, such as HCl, to the solvent may be required to remove RhB. According to the report in the literature, a high desorption efficiency of RhB-loaded Fe_3O_4/MIL-100(Fe) was achieved using methanol as the solvent with the addition of HCl (0.001 mol L^{-1}) [60]. Nevertheless, it can be suggested that MIL-88B adsorption capacities towards both organic dyes are still good after regeneration, which indicates that the as-prepared MOF is completely recyclable.

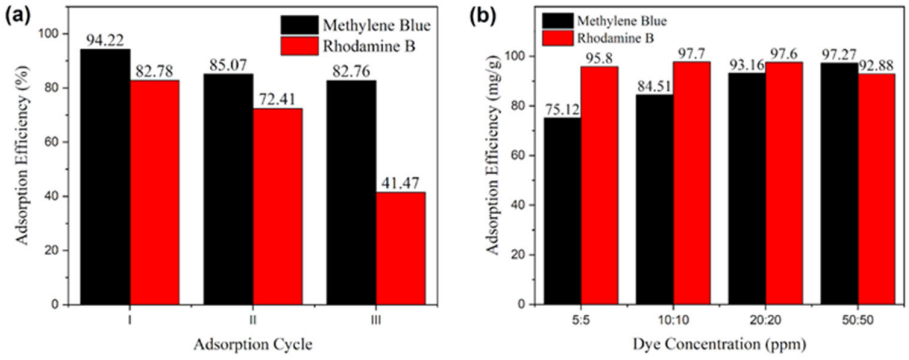

Figure 7. (**a**) Reusability and (**b**) adsorption capabilities of MIL-88B(Fe).

3.2.8. Selective Adsorption Capability

Another crucial aspect of the process of treating dye wastewater was the selective adsorption of the particular dye. The experimental findings in Figure 7b demonstrate that competitive adsorption took place at low concentrations of both cationic dyes. Due to the interaction potency and breathing behaviour of MIL-88B(Fe), RhB was more adsorbable than MB. However, at high concentrations, there was no discernible difference between MB and RhB adsorption. The interaction between the positive and negative charges of the respective dyes and MIL-88B(Fe), which happens electrostatically, affects the adsorption process. The anionic charge on MIL-88B (Fe) influences the adsorption selectivity of cationic dyes. Dyes in binary systems will not conflict with one another while adhering to the MOF.

3.2.9. Comparison with Other Adsorbents

Table 5 summarises several studies on the adsorption of MB and RhB on porous solid materials reported by other research groups. As shown, MIL-88B(Fe) is an applicable adsorbent for the elimination of MB and RhB from aqueous solutions. Compared with other reported MOF materials and conventional adsorbents, the synthesised material has a medium BET surface area value and organic functional groups within the framework, which could be attractive due to its rapid and effective adsorption.

Table 5. Comparison of MB and RhB removal.

No.	Adsorbent	BET Surface Area (m^2/g)	Adsorbate	Reaction Conditions					Ref.
				C_0 (mg/L)	pH	Time (min)	Temp (°C)	q_{max} * (mg/g)	
1	MIL-88B(Fe)	28.37	MB	250	9	180	25	218.94	This work
2	NH_2-MIL-88B(Fe)	163.9	MB	20	3–11	45	35	61.46	[23]
3	MIL-101(Fe)	54.71	MB	200	9	500	25	58.82	[28]
4	Fe_3O_4-activated montmorillonite	147.92	MB	120–1000	7.37	25	20	106.38	[15,16]
5	MIL-88B(Fe)	28.37	RhB	250	9	180	25	167.67	This work
6	MIL-68(Al)	976	RhB	15	6.45	9.9	25	29.32	[29]
7	MIL-125(Ti)	845	RhB	10	7	180	25	59.92	[30]
8	Zirconium-based MOFs	-	RhB	10	7	240	25	67.73	[31]

* q_{max} of Langmuir adsorption isotherm parameter.

3.2.10. Plausible Adsorption Mechanism

The dye adsorption behaviour at various pH levels reflects the adsorption mechanism on the surface of MIL-88B(Fe). At basic pH, the adsorption capacity of MIL-88B(Fe) is higher than under acid conditions for both dyes. Since MB and RhB are basic cationic dyes, they form cations (C^+) and reduced ions (CH^+) in water [61]. While the dyes possess a positive charge, the density of the negatively charged MIL-88B(Fe) increases in the basic solution. The electrostatic interaction between opposite charges (positive and negative) promotes the adsorption of dyes on the external area of MIL-88B(Fe). Binding is also ascribed to the π–π interaction of the aromatic ring on MB and the MIL-88B(Fe) structure, whereas it does not form on RhB due to steric hindrance [27,61]. The plausible adsorption mechanism is depicted in Figure 8.

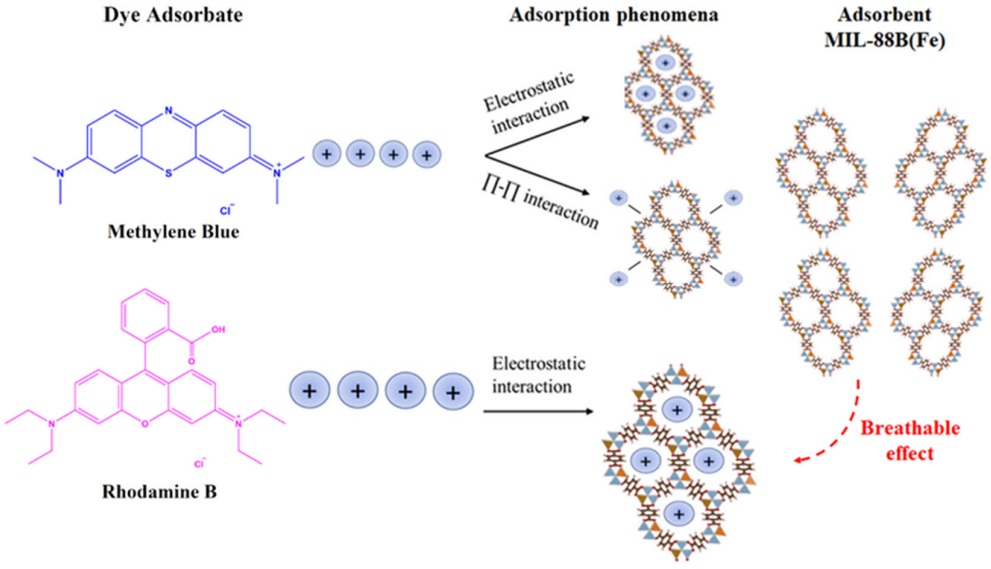

Figure 8. Plausible mechanism of MB and RhB dye adsorption on the surface of MIL-88B(Fe).

Due to the surface-active sites, functional groups, and intraframework interactions that control the flexibility of MIL-88B(Fe), the high adsorption capacity for both cationic dyes was made possible [62]. Firstly, the number of –OH and C=O functional groups in MIL-88B(Fe) plays a crucial role in the adsorption process [27,63]. However, although MIL-88B(Fe) exhibits a larger adsorption capacity of MB in comparison to RhB, their adsorption does not compete with each other in a binary mixture (Figure 8). The high surface area of MIL-88B(Fe) leads to the high adsorption of a binary mixture of MB and RhB. Furthermore, the change in the ΔG° value of RhB at $T > 318$ K confirms the flexibility of the MIL-88B(Fe) framework,

which is in line with the report by Surble et al. The structural flexibility, known as 'the breathing effect', is referred to as a third-generation material by Kitagawa [64,65]. However, the structural breath of the synthesised MOF should be characterised further. Due to the bistable characteristics of MOFs under thermodynamic conditions (such as temperature, pressure, and chemical inclusion), MOFs could exhibit breathable characteristics that could greatly expand their framework, showing their guest-induced feature [37,66]. Furthermore, after three cycles of regeneration, the adsorption capacity of MIL-88B(Fe) for MB remains high, while that for RhB decreases. Based on the plausible mechanism shown in Figure 8, there is a chemical interaction between MIL-88B(Fe) and cationic dyes that is difficult to break by a simple washing method. Although it is quite effective to remove dyes using the simple solvent mixture, a more severe method is needed to separate dyes and MIL-88B(Fe). Therefore, this breathable feature of MIL-88B(Fe) is considered useful to overcome the pore size limitation often faced by adsorbents.

4. Conclusions

The replacement of Cr^{3+} in MIL-101 by Fe^{3+} led to the creation of an MIL-88B(Fe) adsorbent with good crystallinity and a high surface area. MB and RhB adhere to MIL-88B(Fe) in accordance with the Langmuir model, which predicts the one-layer chemisorption of the dyes on the MOF surface. However, the Freundlich model also concurs with the experimental findings of MB and RhB adsorption, suggesting that the bond between both cationic dyes and MIL-88B(Fe) is not entirely monolayer. Due to the breathing effect of the framework, MIL-88B(Fe) demonstrated high adsorption selectivity for both MB and RhB even in mixtures with small concentrations of dye. MIL-88B(Fe) can be reused as an effective adsorbent for removing MB after the third adsorption–desorption experiment, as evidenced by a slight reduction in efficiency. In contrast, due to the significant decrease in RhB adsorption after three cycles, the reusability of MIL-88B(Fe) for RhB adsorption is limited.

Supplementary Materials: The following supporting information can be downloaded at: https://www.mdpi.com/article/10.3390/chemistry6020015/s1. Figure S1: Rietveld refinement of XRD pattern; Figure S2: EDX spectrum; Figure S3: N_2 physisorption graphs; Figure S4: Comparison between linear and nonlinear fitting of the adsorption kinetics.

Author Contributions: Conceptualisation, D.A.N. and Y.K.K.; methodology, D.A.N. and Y.K.K.; formal analysis, N.A., I.K. and Y.; investigation, N.A., I.K. and Y.; writing—original draft preparation, D.A.N. and N.A.; writing—review and editing, N.A., I.K., D.A.N., Y.K.K. and G.T.M.K.; supervision, D.A.N. and Y.K.K.; funding acquisition, Y.K.K. All authors have read and agreed to the published version of the manuscript.

Funding: This research was funded by Universitas Indonesia through Hibah Publikasi Terindeks Internasional (PUTI) Q2 Research Grant No. NKB-670/UN2.RST/HKP.05.00/2022 and the Indonesian Ministry of Research and Technology/National Research and Innovation Agency (Menristek/BRIN) for funding the project with the BOPTN grant for Applied Research No. NKB-294/UN2.RST/HKP.05.00/2020.

Data Availability Statement: The data presented in this study are available upon request from the corresponding author and co-authors.

Conflicts of Interest: The authors declare no conflicts of interest.

References

1. Karmakar, S.; Roy, D.; Janiak, C.; De, S. Insights into Multi-Component Adsorption of Reactive Dyes on MIL-101-Cr Metal Organic Framework: Experimental and Modeling Approach. *Sep. Purif. Technol.* **2019**, *215*, 259–275. [CrossRef]
2. Onu, C.E.; Asadu, C.O.; Ohale, P.E.; Ojukwu, E.V.; Ogunaobi, N.C.; Onu, C.P.; Akaeme, F.C. Recent Trends in Textile Wastewater Treatment Using Agricultural Waste. In *Textile Wastewater Treatment*; Springer: Singapore, 2022; pp. 89–110. [CrossRef]
3. Ghasemi, H.; Aghabarari, B.; Alizadeh, M.; Khanlarkhani, A.; Abu-Zahra, N. High Efficiency Decolorization of Wastewater by Fenton Catalyst: Magnetic Iron-Copper Hybrid Oxides. *J. Water Process Eng.* **2020**, *37*, 101540. [CrossRef]
4. Chiu, Y.H.; Chang, T.F.M.; Chen, C.Y.; Sone, M.; Hsu, Y.J. Mechanistic Insights into Photodegradation of Organic Dyes Using Heterostructure Photocatalysts. *Catalysts* **2019**, *9*, 430. [CrossRef]

5. Demissie, H.; An, G.; Jiao, R.; Ritigala, T.; Lu, S.; Wang, D. Modification of High Content Nanocluster-Based Coagulation for Rapid Removal of Dye from Water and the Mechanism. *Sep. Purif. Technol.* **2021**, *259*, 117845. [CrossRef]
6. Zazou, H.; Afanga, H.; Akhouairi, S.; Ouchtak, H.; Addi, A.A.; Akbour, R.A.; Assabbane, A.; Douch, J.; Elmchaouri, A.; Duplay, J.; et al. Treatment of Textile Industry Wastewater by Electrocoagulation Coupled with Electrochemical Advanced Oxidation Process. *J. Water Process Eng.* **2019**, *28*, 214–221. [CrossRef]
7. Zhu, T.T.; Zhang, Z.M.; Chen, W.L.; Liu, Z.J.; Wang, E.B. Encapsulation of Tungstophosphoric Acid into Harmless MIL-101(Fe) for Effectively Removing Cationic Dye from Aqueous Solution. *RSC Adv.* **2016**, *6*, 81622–81630. [CrossRef]
8. Adeyemo, A.A.; Adeoye, I.O.; Bello, O.S. Metal Organic Frameworks as Adsorbents for Dye Adsorption: Overview, Prospects and Future Challenges. *Toxicol. Environ. Chem.* **2012**, *94*, 1846–1863. [CrossRef]
9. Haque, E.; Jun, J.W.; Jhung, S.H. Adsorptive Removal of Methyl Orange and Methylene Blue from Aqueous Solution with a Metal-Organic Framework Material, Iron Terephthalate (MOF-235). *J. Hazard. Mater.* **2011**, *185*, 507–511. [CrossRef]
10. Lin, S.; Song, Z.; Che, G.; Ren, A.; Li, P.; Liu, C.; Zhang, J. Adsorption Behavior of Metal–Organic Frameworks for Methylene Blue from Aqueous Solution. *Microporous Mesoporous Mater.* **2014**, *193*, 27–34. [CrossRef]
11. Wu, Z.; Chen, C.; Wan, H.; Wang, L.; Li, Z.; Li, B.; Guo, Q.; Guan, G. Fabrication of Magnetic NH2-MIL-88B (Fe) Confined Brønsted Ionic Liquid as an Efficient Catalyst in Biodiesel Synthesis. *Energy Fuels* **2016**, *30*, 10739–10746. [CrossRef]
12. Zhu, G.; Xing, X.; Wang, J.; Zhang, X. Effect of Acid and Hydrothermal Treatments on the Dye Adsorption Properties of Biomass-Derived Activated Carbon. *J. Mater. Sci.* **2017**, *52*, 7664–7676. [CrossRef]
13. Shafqat, S.R.; Bhawani, S.A.; Bakhtiar, S.; Ibrahim, M.N.M. Synthesis of Molecularly Imprinted Polymer for Removal of Congo Red. *BMC Chem.* **2020**, *14*, 27. [CrossRef]
14. Rahimi, B.; Jafari, N.; Abdolahnejad, A.; Farrokhzadeh, H.; Ebrahimi, A. Application of Efficient Photocatalytic Process Using a Novel BiVO/TiO_2-NaY Zeolite Composite for Removal of Acid Orange 10 Dye in Aqueous Solutions: Modeling by Response Surface Methodology (RSM). *J. Environ. Chem. Eng.* **2019**, *7*, 103253. [CrossRef]
15. Chang, J.; Ma, J.; Ma, Q.; Zhang, D.; Qiao, N.; Hu, M.; Ma, H. Adsorption of Methylene Blue onto Fe_3O_4/Activated Montmorillonite Nanocomposite. *Appl. Clay Sci.* **2016**, *119*, 132–140. [CrossRef]
16. Mashkoor, F.; Nasar, A. Magsorbents: Potential Candidates in Wastewater Treatment Technology—A Review on the Removal of Methylene Blue Dye. *J. Magn. Magn. Mater.* **2020**, *500*, 166408. [CrossRef]
17. Zango, Z.U.; Jumbri, K.; Sambudi, N.S.; Hanif Abu Bakar, N.H.; Fathihah Abdullah, N.A.; Basheer, C.; Saad, B. Removal of Anthracene in Water by MIL-88(Fe), NH 2 -MIL-88(Fe), and Mixed-MIL-88(Fe) Metal–Organic Frameworks. *RSC Adv.* **2019**, *9*, 41490–41501. [CrossRef]
18. James, S.L. Metal-Organic Frameworks. *Chem. Soc. Rev.* **2003**, *32*, 276–288. [CrossRef]
19. Britt, D.; Tranchemontagne, D.; Yaghi, O.M. Metal-Organic Frameworks with High Capacity and Selectivity for Harmful Gases. *Proc. Natl. Acad. Sci. USA* **2008**, *105*, 11623–11627. [CrossRef]
20. Liu, X.; Zhou, Y.; Zhang, J.; Tang, L.; Luo, L.; Zeng, G. Iron Containing Metal-Organic Frameworks: Structure, Synthesis, and Applications in Environmental Remediation. *ACS Appl. Mater. Interfaces* **2017**, *9*, 20255–20275. [CrossRef]
21. Li, C.; Xiong, Z.; Zhang, J.; Wu, C. The Strengthening Role of the Amino Group in Metal-Organic Framework MIL-53 (Al) for Methylene Blue and Malachite Green Dye Adsorption. *J. Chem. Eng. Data* **2015**, *60*, 3414–3422. [CrossRef]
22. Fu, Q.; Lou, J.; Zhang, R.; Peng, L.; Zhou, S.; Yan, W.; Mo, C.; Luo, J. Highly Effective and Fast Removal of Congo Red from Wastewater with Metal-Organic Framework Fe-MIL-88NH2. *J. Solid State Chem.* **2021**, *294*, 121836. [CrossRef]
23. He, J.; Zhang, Y.; Zhang, X.; Huang, Y. Highly Efficient Fenton and Enzyme-Mimetic Activities of NH2-MIL-88B(Fe) Metal Organic Framework for Methylene Blue Degradation. *Sci. Rep.* **2018**, *8*, 5159. [CrossRef]
24. Uddin, M.J.; Ampiaw, R.E.; Lee, W. Adsorptive Removal of Dyes from Wastewater Using a Metal-Organic Framework: A Review. *Chemosphere* **2021**, *284*, 131314. [CrossRef]
25. Abbasi, A.R.; Karimi, M.; Daasbjerg, K. Efficient Removal of Crystal Violet and Methylene Blue from Wastewater by Ultrasound Nanoparticles Cu-MOF in Comparison with Mechanosynthesis Method. *Ultrason. Sonochem.* **2017**, *37*, 182–191. [CrossRef]
26. Zhang, J.; Li, F.; Sun, Q. Rapid and Selective Adsorption of Cationic Dyes by a Unique Metal-Organic Framework with Decorated Pore Surface. *Appl. Surf. Sci.* **2018**, *440*, 1219–1226. [CrossRef]
27. Ghosh, A.; Das, G. Green Synthesis of Sn(II)-BDC MOF: Preferential and Efficient Adsorption of Anionic Dyes. *Microporous Mesoporous Mater.* **2020**, *297*, 110039. [CrossRef]
28. Eltaweil, A.S.; Abd El-Monaem, E.M.; Omer, A.M.; Khalifa, R.E.; Abd El-Latif, M.M.; El-Subruiti, G.M.; Omer, A.M. Efficient Removal of Toxic Methylene Blue (MB) Dye from Aqueous Solution Using a Metal-Organic Framework (MOF) MIL-101(Fe): Isotherms, Kinetics, and Thermodynamic Studies. *Desalination Water Treat.* **2020**, *189*, 395–407. [CrossRef]
29. Saghanejhad Tehrani, M.; Zare-Dorabei, R. Highly Efficient Simultaneous Ultrasonic-Assisted Adsorption of Methylene Blue and Rhodamine B onto Metal Organic Framework MIL-68(Al): Central Composite Design Optimization. *RSC Adv.* **2016**, *6*, 27416–27425. [CrossRef]
30. Guo, H.; Lin, F.; Chen, J.; Li, F.; Weng, W. Metal–Organic Framework MIL-125(Ti) for Efficient Adsorptive Removal of Rhodamine B from Aqueous Solution. *Appl. Organomet. Chem.* **2015**, *29*, 12–19. [CrossRef]
31. Zhao, J.; Xu, L.; Su, Y.; Yu, H.; Liu, H.; Qian, S.; Zheng, W.; Zhao, Y. Zr-MOFs Loaded on Polyurethane Foam by Polydopamine for Enhanced Dye Adsorption. *J. Environ. Sci.* **2021**, *101*, 177–188. [CrossRef] [PubMed]

32. Agustin, M.; Nurani, D.A.; Zulys, A.; Krisnandi, Y.K. Adsorption of Rhodamine B by Yttrium-Succinate Metal Organic Framework (MOF). *AIP Conf. Proc.* **2020**, *2243*, 030001. [CrossRef]
33. Nurani, D.A.; Butar, B.C.B.; Krisnandi, Y.K. Synthesis and Characterization of Metal Organic Framework Using Succinic Acid Ligand with Cobalt and Iron Metals as Methylene Blue Dye Adsorbent. *IOP Conf. Ser. Mater. Sci. Eng.* **2020**, *902*, 012055. [CrossRef]
34. Knyazeva, M.K.; Shkolin, A.V.; Fomkin, A.A.; Tsivadze, A.Y.; Solovtsova, O.V.; Platonova, N.P.; Pulin, A.L.; Men'shchikov, I.E.; Shiryaev, A.A.; Vysotskii, V.V.; et al. Synthesis and Structural-Energy Characteristics of Fe-BDC Metal-Organic Frameworks. *Prot. Met. Phys. Chem. Surf.* **2018**, *54*, 1004–1009. [CrossRef]
35. Pertiwi, R.; Oozeerally, R.; Burnett, D.L.; Chamberlain, T.W.; Cherkasov, N.; Walker, M.; Kashtiban, R.J.; Krisnandi, Y.K.; Degirmenci, V.; Walton, R.I. Replacement of Chromium by Non-Toxic Metals in Lewis-Acid MOFs: Assessment of Stability as Glucose Conversion Catalysts. *Catalysts* **2019**, *9*, 437. [CrossRef]
36. Wu, L.; Chaplais, G.; Xue, M.; Qiu, S.; Patarin, J.; Simon-Masseron, A.; Chen, H. New Functionalized MIL-53(In) Solids: Syntheses, Characterization, Sorption, and Structural Flexibility. *RSC Adv.* **2019**, *9*, 1918–1928. [CrossRef]
37. Wei, Y.S.; Chen, K.J.; Liao, P.Q.; Zhu, B.Y.; Lin, R.B.; Zhou, H.L.; Wang, B.Y.; Xue, W.; Zhang, J.P.; Chen, X.M. Turning on the Flexibility of Isoreticular Porous Coordination Frameworks for Drastically Tunable Framework Breathing and Thermal Expansion. *Chem. Sci.* **2013**, *4*, 1539–1546. [CrossRef]
38. Chaplais, G.; Simon-Masseron, A.; Porcher, F.; Lecomte, C.; Bazer-Bachi, D.; Bats, N.; Patarin, J. IM-19: A New Flexible Microporous Gallium Based-MOF Framework with Pressure- and Temperature-Dependent Openings. *Phys. Chem. Chem. Phys.* **2009**, *11*, 5241–5245. [CrossRef]
39. Volkringer, C.; Loiseau, T.; Guillou, N.; Férey, G.; Elkaïm, E.; Vimont, A. XRD and IR Structural Investigations of a Particular Breathing Effect in the MOF-Type Gallium Terephthalate MIL-53(Ga). *Dalton Trans.* **2009**, 2241–2249. [CrossRef]
40. Surblé, S.; Serre, C.; Mellot-Draznieks, C.; Millange, F.; Férey, G. A New Isoreticular Class of Metal-Organic-Frameworks with the MIL-88 Topology. *Chem. Commun.* **2006**, 284–286. [CrossRef]
41. Toby, B.H. R Factors in Rietveld Analysis: How Good Is Good Enough? *Powder Diffr.* **2006**, *21*, 67–70. [CrossRef]
42. Carson, F.; Su, J.; Platero-Prats, A.E.; Wan, W.; Yun, Y.; Samain, L.; Zou, X. Framework Isomerism in Vanadium Metal-Organic Frameworks: MIL-88B(V) and MIL-101(V). *Cryst. Growth Des.* **2013**, *13*, 5036–5044. [CrossRef]
43. Dhanapala, B.D.; Maglich, D.L.; Anderson, M.E. Impact of Surface Functionalization and Deposition Method on Cu-BDC SurMOF Formation, Morphology, Crystallinity, and Stability. *Langmuir* **2023**, *39*, 12196–12205. [CrossRef] [PubMed]
44. Taylor-Pashow, K.M.L.; Della Rocca, J.; Xie, Z.; Tran, S.; Lin, W. Postsynthetic Modifications of Iron-Carboxylate Nanoscale Metal-Organic Frameworks for Imaging and Drug Delivery. *J. Am. Chem. Soc.* **2009**, *131*, 14261–14263. [CrossRef]
45. Rahmani, E.; Rahmani, M. Alkylation of Benzene over Fe-Based Metal Organic Frameworks (MOFs) at Low Temperature Condition. *Microporous Mesoporous Mater.* **2017**, *249*, 118–127. [CrossRef]
46. Vuong, G.T.; Pham, M.H.; Do, T.O. Synthesis and Engineering Porosity of a Mixed Metal Fe_2Ni MIL-88B Metal–Organic Framework. *Dalton Trans.* **2012**, *42*, 550–557. [CrossRef] [PubMed]
47. Zou, M.; Dong, M.; Zhao, T. Advances in Metal-Organic Frameworks MIL-101(Cr). *Int. J. Mol. Sci.* **2022**, *23*, 9396. [CrossRef]
48. Shen, T.; Luo, J.; Zhang, S.; Luo, X. Hierarchically Mesostructured MIL-101 Metal–Organic Frameworks with Different Mineralizing Agents for Adsorptive Removal of Methyl Orange and Methylene Blue from Aqueous Solution. *J. Environ. Chem. Eng.* **2015**, *3*, 1372–1383. [CrossRef]
49. Zhao, T.; Zhu, H.; Dong, M.; Zou, M.; Tang, S.; Luo, M.; Li, X. Low-Temperature and Additive-Free Synthesis of Spherical MIL-101(Cr) with Enhanced Dye Adsorption Performance. *Inorganics* **2022**, *10*, 33. [CrossRef]
50. Vo, T.K.; Trinh, T.P.; Nguyen, V.C.; Kim, J. Facile Synthesis of Graphite Oxide/MIL-101(Cr) Hybrid Composites for Enhanced Adsorption Performance towards Industrial Toxic Dyes. *J. Ind. Eng. Chem.* **2021**, *95*, 224–234. [CrossRef]
51. Tan, Y.; Sun, Z.; Meng, H.; Han, Y.; Wu, J.; Xu, J.; Xu, Y.; Zhang, X. Efficient and Selective Removal of Congo Red by Mesoporous Amino-Modified MIL-101(Cr) Nanoadsorbents. *Powder Technol.* **2019**, *356*, 162–169. [CrossRef]
52. Hidalgo, T.; Alonso-Nocelo, M.; Bouzo, B.L.; Reimondez-Troitiño, S.; Abuin-Redondo, C.; De La Fuente, M.; Horcajada, P. Biocompatible Iron(III) Carboxylate Metal–Organic Frameworks as Promising RNA Nanocarriers. *Nanoscale* **2020**, *12*, 4839–4845. [CrossRef]
53. Revellame, E.D.; Fortela, D.L.; Sharp, W.; Hernandez, R.; Zappi, M.E. Adsorption Kinetic Modeling Using Pseudo-First Order and Pseudo-Second Order Rate Laws: A Review. *Clean. Eng. Technol.* **2020**, *1*, 100032. [CrossRef]
54. Zhang, G.; Wo, R.; Sun, Z.; Hao, G.; Liu, G.; Zhang, Y.; Guo, H.; Jiang, W. Effective Magnetic Mofs Adsorbent for the Removal of Bisphenol a, Tetracycline, Congo Red and Methylene Blue Pollutions. *Nanomaterials* **2021**, *11*, 1917. [CrossRef] [PubMed]
55. Wang, X.; Jiang, C.; Hou, B.; Wang, Y.; Hao, C.; Wu, J. Carbon Composite Lignin-Based Adsorbents for the Adsorption of Dyes. *Chemosphere* **2018**, *206*, 587–596. [CrossRef] [PubMed]
56. Yadav, M.; Thakore, S.; Jadeja, R. Removal of Organic Dyes Using Fucus Vesiculosus Seaweed Bioadsorbent an Ecofriendly Approach: Equilibrium, Kinetics and Thermodynamic Studies. *Environ. Chem. Ecotoxicol.* **2022**, *4*, 67–77. [CrossRef]
57. Kundu, A.; Mondal, A. Kinetics, Isotherm, and Thermodynamic Studies of Methylene Blue Selective Adsorption and Photocatalysis of Malachite Green from Aqueous Solution Using Layered Na-Intercalated Cu-Doped Titania. *Appl. Clay Sci.* **2019**, *183*, 105323. [CrossRef]
58. Konicki, W.; Hełminiak, A.; Arabczyk, W.; Mijowska, E. Adsorption of Cationic Dyes onto Fe@graphite Core–Shell Magnetic Nanocomposite: Equilibrium, Kinetics and Thermodynamics. *Chem. Eng. Res. Des.* **2018**, *129*, 259–270. [CrossRef]

59. Feng, M.; Yu, S.; Wu, P.; Wang, Z.; Liu, S.; Fu, J. Rapid, High-Efficient and Selective Removal of Cationic Dyes from Wastewater Using Hollow Polydopamine Microcapsules: Isotherm, Kinetics, Thermodynamics and Mechanism. *Appl. Surf. Sci.* **2021**, *542*, 148633. [CrossRef]
60. Liu, H.; Ren, X.; Chen, L. Synthesis and Characterization of Magnetic Metal–Organic Framework for the Adsorptive Removal of Rhodamine B from Aqueous Solution. *J. Ind. Eng. Chem.* **2016**, *34*, 278–285. [CrossRef]
61. Arora, C.; Soni, S.; Sahu, S.; Mittal, J.; Kumar, P.; Bajpai, P.K. Iron Based Metal Organic Framework for Efficient Removal of Methylene Blue Dye from Industrial Waste. *J. Mol. Liq.* **2019**, *284*, 343–352. [CrossRef]
62. Yilmaz, E.; Sert, E.; Atalay, F.S. Synthesis, Characterization of a Metal Organic Framework: MIL-53 (Fe) and Adsorption Mechanisms of Methyl Red onto MIL-53 (Fe). *J. Taiwan Inst. Chem. Eng.* **2016**, *65*, 323–330. [CrossRef]
63. Devic, T.; Horcajada, P.; Serre, C.; Salles, F.; Maurin, G.; Moulin, B.; Heurtaux, D.; Clet, G.; Vimont, A.; Grenéche, J.M.; et al. Functionalization in Flexible Porous Solids: Effects on the Pore Opening and the Host-Guest Interactions. *J. Am. Chem. Soc.* **2010**, *132*, 1127–1136. [CrossRef]
64. Uemura, K.; Matsuda, R.; Kitagawa, S. Flexible Microporous Coordination Polymers. *J. Solid State Chem.* **2005**, *178*, 2420–2429. [CrossRef]
65. Fletcher, A.J.; Thomas, K.M.; Rosseinsky, M.J. Flexibility in Metal-Organic Framework Materials: Impact on Sorption Properties. *J. Solid State Chem.* **2005**, *178*, 2491–2510. [CrossRef]
66. Long, J.; Yaghi, O.; Ge'rard, G.; Férey, F.; Serre, C. Large Breathing Effects in Three-Dimensional Porous Hybrid Matter: Facts, Analyses, Rules and Consequences. *Chem. Soc. Rev.* **2009**, *38*, 1380–1399. [CrossRef]